Green Chemistry

PAPER

View Article Online
View Journal | View Issue

Open Access Article. Published on 27 March 2025. Downloaded on 11/8/2025 10:42:49 AM.
This article is licensed under a Creative Commons Attribution-NonCommercial 3.0 Unported Licence.

Check for updates

Cite this: *Green Chem.*, 2025, **27**, 4587

Full conversion of grass biomass into sustainable functional antimicrobial bioplastics†

José David Estrada-Sotomayor,[a] Łukasz Łopusiewicz,[b,c] Erlantz Lizundia,[d,e] Sebastian Guenther[c] and Danila Merino *[a,f]

Received 6th February 2025,
Accepted 27th March 2025

DOI: 10.1039/d5gc00643k

rsc.li/greenchem

The environmental impact of non-degradable single-use plastics poses a significant challenge to current sustainability efforts. To foster a sustainable circular economy, this study introduces grass biomass as a renewable resource for the production of innovative bioplastics. The research involves the direct conversion of grass waste into composite bioplastics through alkaline hydrolysis, offering a transformative approach to plastic manufacturing. The hydrolysis process was optimized by varying treatment times and alkaline concentrations, with the ideal conditions identified as 1 M NH_3 and 24 hours of treatment. Subsequently, the incorporation of ε-polylysine (PL) enhanced the mechanical properties of the bioplastics by acting as a plasticizer. Mechanical testing revealed that samples containing 10% and 20% PL exhibited comparable rigidity, with a Young's modulus of approximately 700 MPa and a tensile strength of 10 MPa. Moreover, the addition of PL, up to 20%, significantly improved the water resistance of the bioplastics, evidenced by decreased moisture content and water solubility. Additionally, the bioplastics demonstrated effective antimicrobial activity against *Escherichia coli* and *Staphylococcus aureus*, as well as significant antioxidant activity. Life cycle assessment (LCA) and life cycle costing (LCAA) results demonstrate the potential environmental benefits of manufacturing grass biomass into plastic films, with a significant reduction in greenhouse gases, cumulative energy demand (CED), and cost when compared to benchmark packaging plastics. These promising properties indicate that these biomaterials could be effectively utilized in real-world applications, with potential application as sustainable biobased packaging materials.

Green foundation

1. Our work advances green chemistry by introducing a solvent-minimized process to transform grass biomass into functional bioplastics. This approach eliminates the need for intensive chemical extractions, reduces waste, and enhances material performance through a single-step hydrolysis method.
2. Our bioplastics achieve a cradle-to-gate carbon footprint of 1.69 kg CO_2 per kg, significantly lower than PLA (3.40 kg CO_2 per kg) and polyethylene terephthalate (PET) (3.62 kg CO_2 per kg). The process utilizes mild alkaline hydrolysis instead of organic solvents, cutting down hazardous waste. The resulting materials are fully bio-based, biodegradable, antimicrobial, and antioxidant, reducing the need for synthetic additives and preservatives.
3. Future research could focus on recycling ammonia from the hydrolysis process to further reduce environmental impact. Additionally, scaling up production with renewable energy sources and optimizing biopolymer interactions could enhance both the sustainability and functionality of these materials.

1. Introduction

With over 400 million metric tonnes produced globally in 2023, plastics have become essential in everyday life.[1,2] Their high tunability in terms of mechanical, barrier or thermal properties makes them especially valuable in the packaging industry, where they dominate due to their versatility.[3] Lightweight polymers such as polyethylene (PE), polyethylene terephthalate (PET), and polycarbonate (PC) are commonly used in packaging for their excellent mechanical strength, barrier properties, and resistance to chemical and environmental degradation.[4,5] However, the same durability and resistance to degradation that make these materials so valuable have also become significant environmental issues, especially in the context of single-use plastics.[6]

[a]*Basque Center for Macromolecular Design and Engineering (POLYMAT), University of the Basque Country (UPV/EHU), Avenida de Tolosa 72, 20018 Donostia-San Sebastian, Spain. E-mail: danila.merino@ehu.eus*
[b]*School of Medical & Health Sciences, University of Economics and Human Sciences in Warsaw, 59 Okopowa Str., Warszawa, 01-043, Poland*
[c]*Institute of Pharmacy, Department Pharmaceutical Biology, Greifswald University, Friedrich-Ludwig-Jahn-Str. 17, 17489 Greifswald, Germany*
[d]*Life Cycle Thinking Group, Department of Graphic Design and Engineering Projects, Faculty of Engineering in Bilbao. University of the Basque Country (UPV/EHU), Bilbao, 48013, Spain*
[e]*BCMaterials, Basque Center for Materials, Applications and Nanostructures, UPV/EHU Science Park, Leioa, 48940, Spain*
[f]*Ikerbasque, Basque Foundation for Science, 48009 Bilbao, Spain*
† Electronic supplementary information (ESI) available. See DOI: https://doi.org/10.1039/d5gc00643k

Open Access Article. Published on 27 March 2025. Downloaded on 11/8/2025 10:42:49 AM.
This article is licensed under a Creative Commons Attribution-NonCommercial 3.0 Unported Licence.

In Europe, nearly one in four plastic items ends up in landfills, contributing to the accumulation of post-consumer plastic waste.[7] This waste degrades soil quality,[2] generates micro- and nanoplastics,[8,9] and poses threats to human health[10] and agricultural productivity.[11] Plastic waste in landfills also risks leaching into water bodies, harming aquatic ecosystems,[2] causing bioaccumulation of hazardous substances,[12] and releasing toxic additives into the oceans.[12] These escalating environmental challenges underscore the urgent need for sustainable alternatives. One proposed solution is a transition to a circular economy.

A key aspect of this shift is the development of bioplastics as alternatives to conventional plastics.[13] Among potential raw materials, lignocellulosic biomass stands out as particularly promising. An estimated 1.3 billion tonnes of this biomass, rich in cellulose (40–60 wt%), hemicellulose (20–40 wt%), and lignin (10–24 wt%), are generated annually around the globe. Furthermore, much of this biomass is available as waste from various industries. However, current studies on bioplastics derived from lignocellulosic biomass tend to focus on extracting macromolecules such as cellulose and lignin by using organic solvents and energy-intensive processes that compromise long-term sustainability.[14] These approaches also isolate specific components, leaving residues and underutilizing the full potential of the biomass.

Recent research has explored hydrolysis-based processes as a greener alternative for converting biomass such as spinach stems, citrus peels, and carrot pomace into bioplastic films with desirable properties.[15–19] This process involves partial hydrolysis of lignin, pectin and hemicellulose, disrupting plant cell walls and releasing cellulose nano- and microfibers, which are regenerated into a composite material. In these composites, cellulose nanofibrils are embedded within an amorphous polymer matrix.[15] While these biomass-derived bioplastics exhibit good mechanical properties and thermal stability, film formation success depends on the raw material composition. For instance, peanut shells, despite forming continuous films, resulted in highly brittle materials, likely do to their low hemicellulose content.[19] Additionally, these bioplastics often degrade rapidly due to their high hydrophilicity and susceptibility to microbial attack, highlighting challenges that require further optimization.

Furthermore, life cycle assessment (LCA) and life cycle costing (LCC) results are valuable to confirm that the attributes of environmental and economic sustainability, which include the use of naturally derived materials and straightforward processing with low energy and chemical requirements, are translated in materials with low environmental impact.[20,21] Furthermore, LCA enables the determination of the environmental hotspots during the product's lifecycle, allowing the eco-design the material to enhance sustainability.[22]

In this study, *Brachiaria decumbens* grass was selected as the starting biomass, given its abundance as a non-edible resource and its global availability. Though grass is primarily used for biofuel production,[23,24] its potential for bioplastic development remains underexplored. To enhance the performance of these bioplastics, ε-polylysine (PL), a biopolymer known for its antimicrobial properties, was incorporated into the formulation. Recent advancements have improved the production efficiency of PL, making it more cost-effective.[25] As a homopolymer of amino acids, PL consists of 25–35 lysine residues connected by peptide bonds between the ε-amino and α-carboxylic groups,[26] offering water solubility and biodegradability, which makes it compatible with the alkaline media used in grass-derived bioplastic preparation.[19]

However, due to its low molecular weight, PL alone cannot produce high-quality films.[27] To overcome this limitation, crosslinking PL with reducing sugars through Schiff base formation has been investigated.[28] This strategy aims to enhance the mechanical properties, flexibility, and insolubility of the bioplastics.[27,28] Since hydrolysis of lignocellulosic biomass produces reducing sugars, exploring their potential for crosslinking with PL to develop high-quality, ductile films with antimicrobial properties is of significant interest.

The objective of this study is to develop a novel bioplastic from underutilized *Brachiaria decumbens* grass biomass as a sustainable alternative to conventional plastics in packaging applications. We have optimized the conditions for alkaline hydrolysis of grass to produce bioplastics with enhanced mechanical properties. Additionally, PL was incorporated to impart antimicrobial properties. The bioplastics were characterized in terms of their physicochemical, morphological, optical, mechanical, and barrier properties. Furthermore, their antibacterial efficacy was tested against *Escherichia coli* (*E. coli*) and *Staphylococcus aureus* (*S. aureus*), two common pathogens affecting both human health and food safety. The antioxidant properties of the materials were also evaluated to assess potential applicability in food contact materials, including cutlery, trays, and fast-food packaging.

2. Materials and methods

2.1 Materials

PL of 95% purity was purchased from BLDpharm. Ammonium hydroxide of ~30–33% NH_3 in H_2O was purchased from Fluka. $NaClO_2$ purity of 80% was purchased from Sigma Aldrich. The grass biomass was manually collected from a public park in San Sebastian, Spain.

2.2 Grass biomass pre-treatment

Cut grass biomass was rinsed with water to remove any possible impurities and was dried in an oven at 60 °C until friable consistency. The dried leaves were blended in an AMZCHEF "professional blender" at high intensity for two cycles. The obtained powder was later sieved in an Endecotts™ MIN200 (London, UK) sieve to obtain particle sizes of <53 μm. The resulting powder was stored at room temperature in a PE bag to avoid humidification and placed away from the sun to prevent any degradation.

 This journal is © The Royal Society of Chemistry 2025

Open Access Article. Published on 27 March 2025. Downloaded on 11/8/2025 10:42:49 AM.
This article is licensed under a Creative Commons Attribution-NonCommercial 3.0 Unported Licence.

2.3 Optimization of the hydrolysis process

Alkaline hydrolysis was selected as the treatment for the biomass, since cellulose micro- and nano-fibrillation has been reported at this condition.[19] The hydrolysis consisted of the treatment of 1 g of biomass with 20 mL of ammonium hydroxide at 40 °C for various durations. To determine the optimal hydrolysis conditions, different concentrations of ammonium hydroxide were tested: 0.1, 0.5, 1, and 2 M, along with varying treatment times: 8, 24, and 43 h. Table 1 provides a summary of samples' name according to the hydrolysis conditions tested. Following the hydrolysis treatment, the solutions were cast onto polytetrafluoroethylene (PTFE) Petri dishes, and the solvent was left to evaporate, forming bioplastic films. A scheme of the procedure to obtain the hydrolysed grass films can be seen in Fig. 1A.

2.4 Bioplastics preparation

Once the optimal hydrolysis conditions were established, bioplastics were prepared by incorporating PL at concentrations of 10, 20, and 30 wt% to act as an antimicrobial agent. These bioplastics were designated as GPL10, GPL20, and GPL30, respectively, as shown in Table 1. PL was added to the formulation before the introduction of ammonium hydroxide.

2.5 Characterization of bioplastics

2.5.1 Polymer content in the biomass. The macromolecular composition of the biomass was analysed, focusing on the quantification of its three primary components: hemicellulose, cellulose, and lignin.

To quantify the holocellulose (HoC) content, that is, the content of hemicellulose and cellulose biopolymers a modified version of Wise's method for non-woody biomasses was utilized.[29] In this procedure, 2 g of biomass were added to an Erlenmeyer flask with 150 mL of deionized H_2O and 1.08 mL of glacial acetic acid. The mixture was heated to 96 °C and stirred for 90 minutes. After heating, the solution was cooled in a refrigerator for 1 hour. Subsequently, the mixture was centrifuged at 15 000*g* for 10 minutes, the supernatant was discarded, and the pellets were placed in an oven at 110 °C overnight to remove excess water. The percentage of HoC was calculated with the following equation:

$$\mathrm{HoC}\,(\%) = \frac{F_{\mathrm{H}} - F_{\mathrm{i}}}{B} \times 100\% \tag{1}$$

where F_{H} is the falcon weight after drying, F_{i} is the initial weight of the empty falcon, and B is the weight of the grass sample.

Hemicellulose (HC) was removed from holocellulose by diluted acid hydrolysis using hydrochloric acid.[30] The extracted holocellulose was treated for 2 h under reflux with 45 mL of HCl at 1 M. Once cooled it was centrifuged at 10 000*g* for 10 min, the supernatant was discarded, and the solid was cleaned with warm water (approx. 50 °C) and centrifuged again at the same conditions. The falcons were placed in an oven at 110 °C overnight and the following equations were used to determine cellulose and hemicellulose content in biomass:

$$C\,(\%) = \mathrm{HoC}\,(\%) \times \frac{F_{\mathrm{c}} - F_{\mathrm{i}}}{H} \tag{2}$$

$$\mathrm{HC}\,(\%) = \mathrm{HoC}\,(\%\ ) \times \left(1 - \frac{F_{\mathrm{c}} - F_{\mathrm{i}}}{H}\right) \tag{3}$$

where F_{c} is the falcon with dried cellulose, F_{i} is the falcon's initial weight, and H is the weight of the HoC sample.

At last, the acid-insoluble lignin (AL) was determined by the method proposed by Ioelovich.[30] According to this method, 0.3 g of biomass was hydrolysed at room temperature using 72 wt% H_2SO_4 for 2 h. After this period, the acid was diluted with 45 mL of distilled water and heated at boiling temperature under reflux for 2 h. After reflux, the solution was refrigerated for 30 min, and centrifuged at 10 000*g* for 10 min. The precipitate was washed with distilled water and placed in an oven at 110 °C until constant weight. The following equation was used to determine the lignin percentage in biomass:

$$\mathrm{AL}\,(\%) = \frac{F_{\mathrm{L}} - F_{\mathrm{i}}}{S} \times 100\% \tag{4}$$

where F_{L} is the falcon weight with the dried sample, F_{i} is the initial weight of the falcon and S is the weight of the starting sample.

2.5.2 Fourier-transform infrared spectroscopy (FTIR). FTIR spectra were obtained using a Bruker Alpha (Billerica, USA) spectrophotometer in attenuated total reflectance (ATR) mode. The measurements were acquired after 24 scans in the range of 4000–400 cm^{-1}, with a resolution of 4 cm^{-1}. Baseline correction and normalisation were done using OPUS software.

2.5.3 Scanning electron microscopy (SEM). The film cross section was analysed using the Hitachi TM3030Plus (Tokyo, Japan) at 15 kV. The films were cryo-fractured in liquid N_2, and the fracture surface was exposed by attaching the film to an aluminium stub with conductive carbon tape. The films were coated with gold for 30 seconds at 30 mA.

Table 1 Bioplastics name, composition and preparation conditions

Sample name	Grass (g)	PL (g)	NH_3 (mL)	NH_3 concentration (M)	Hydrolysis time (h)
G0.18	1	—	20	0.1	8
G0.58	1	—	20	0.5	8
G18	1	—	20	1	8
G28	1	—	20	2	8
G0.124	1	—	20	0.1	24
G0.524	1	—	20	0.5	24
G124	1	—	20	1	24
G224	1	—	20	2	24
G0.143	1	—	20	0.1	43
G0.543	1	—	20	0.5	43
G143	1	—	20	1	43
G243	1	—	20	2	43
GPL10	0.9	0.1	20	1	24
GPL20	0.8	0.2	20	1	24
GPL30	0.7	0.3	20	1	24

Open Access Article. Published on 27 March 2025. Downloaded on 11/8/2025 10:42:49 AM.
This article is licensed under a Creative Commons Attribution-NonCommercial 3.0 Unported Licence.

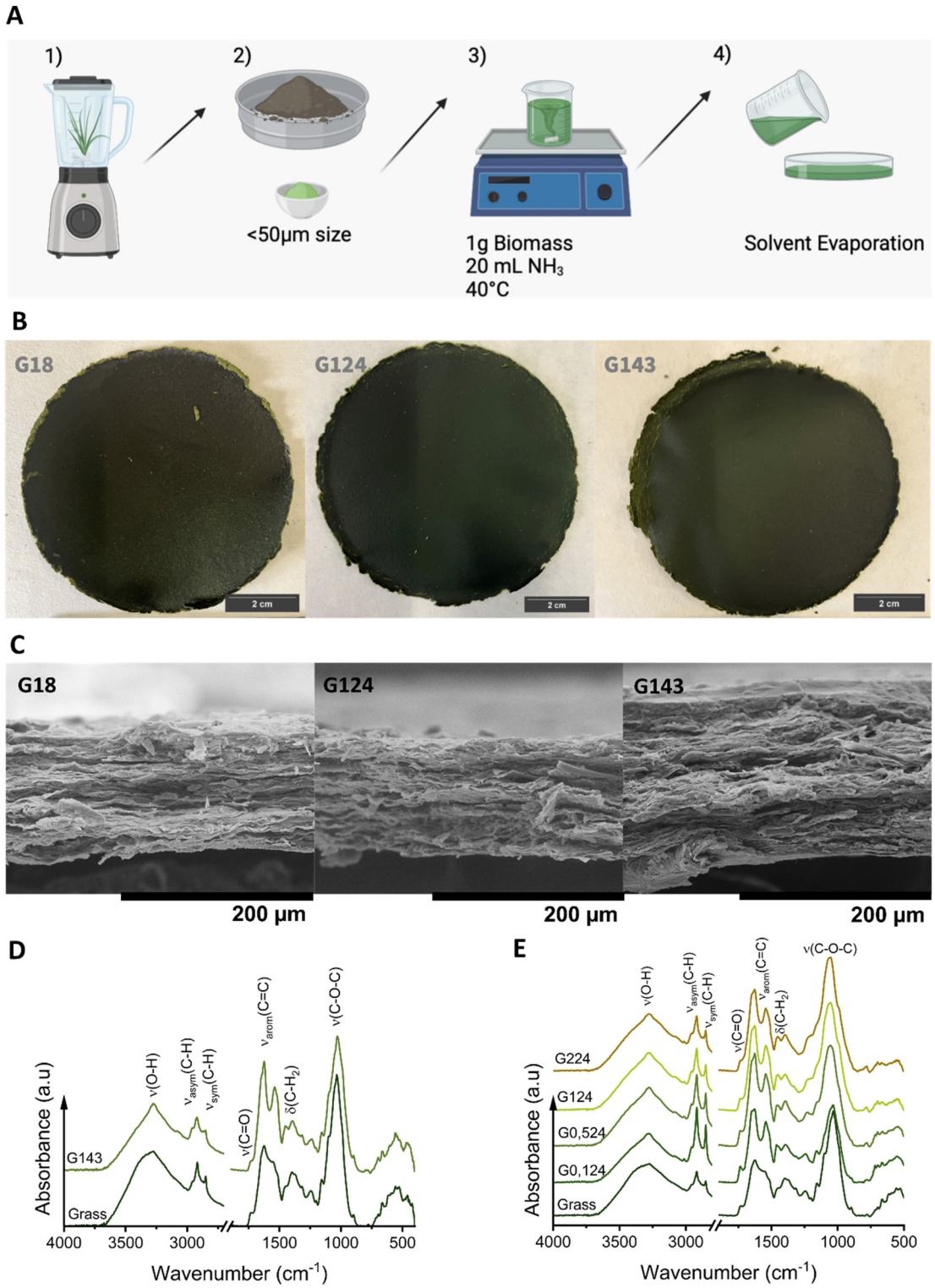

Fig. 1 Preparation, physicochemical and morphological analysis of bioplastic films from *Brachiaria decumbens* grass. (A) Schematic representation of the film preparation process; (B) bioplastic films produced after varying alkaline hydrolysis times at 1 M NH_3; (C) SEM micrographs showing the fracture surfaces of bioplastic films; (D) FTIR peak assignments highlighting the differences between non-hydrolysed and hydrolysed grass; (E) FTIR spectra at different NH_3 concentration at 24 h of hydrolysis.

 This journal is © The Royal Society of Chemistry 2025

Open Access Article. Published on 27 March 2025. Downloaded on 11/8/2025 10:42:49 AM.
This article is licensed under a Creative Commons Attribution-NonCommercial 3.0 Unported Licence.

2.5.4 Mechanical properties. Films were conditioned for at least 48 h at 23 °C in a conditioning room at 50% RH. The tensile tests were performed with the Stable Micro Systems Texture Analyser TA-HD plus (Surrey, UK), with a drawing speed of 0.2 mm sec^{-1}. At least six specimens were tested for each sample, and their Young's modulus (MPa), tensile strength (MPa), and elongation at break (%) were registered using the resulting stress vs strain curves.

2.5.5 Differential scanning calorimetry (DSC). The glass transition temperatures (T_g) of the bioplastics were determined using the TA DSC 2500 (New Castle, USA). Bioplastic films containing PL were heated from −50 °C to 100 °C, with a heating ramp of 10 °C min^{-1} under N_2 atmosphere. A first heating cycle was done to erase any possible thermal history and remove any water present in the sample. The T_g was calculated using the curve obtained after the second heating cycle, and the value for the transition temperature was determined with TRIOS software.

2.5.6 Thermogravimetric analysis (TGA). A PerkinElmer TGA8000 (Waltham, USA) was used to obtain the thermal degradation curves and derivative TGA curves for the hydrolysed grass films and the bioplastic films. Samples were heated from 40 °C to 800 °C, at a heating rate of 10 °C min^{-1} under a N_2 atmosphere, while the sample's mass loss was registered.

2.5.7 Reducing sugars content (RSC). Approximately 0.05 g of the bioplastic samples were placed in 5 mL of distilled water and incubated with shaking at 200 rpm for 1 hour. After incubation, the samples were centrifuged at 4000 rpm for 5 minutes to obtain clear supernatants, which were used for further analyses. The reducing sugars content (RSC) was determined using the 3,5-dinitrosalicylic acid (DNS) method, with a slight modification based on previously reported protocols.[31]

To prepare the DNS working reagent, 10 g of DNS was dissolved in 200 mL of distilled water with continuous stirring. Next, 16 g of NaOH was dissolved in 150 mL of distilled water and slowly added to DNS solution. This mixture was incubated at 50 °C with constant stirring until a clear solution was obtained. Subsequently, 403 g of sodium potassium tartrate tetrahydrate was added to the DNS/NaOH mixture, which was filtered through filter paper. The final volume of the mixture was adjusted to 1000 mL with distilled water.

For the assay, 1 mL of each extract was mixed with 1 mL of 0.05 M acetate buffer (pH 4.8), followed by the addition of 3 mL of DNS working reagent. Then, the mixture was vigorously shaken and incubated in boiling water for 5 minutes, afterward cooled to room temperature. The samples were transferred to a 96-well microplate, and absorbance was measured at 540 nm using a BMG Labtech Clariostar Plus microplate reader (Ortenberg, Germany). A glucose standard prepared in acetate buffer was used to generate the calibration curve.

2.5.8 Moisture content (MC). The moisture content of the films was calculated gravimetrically. Before measurements, all samples were conditioned for 24 h in a conditioning room at 50% RH at 23 °C. The weight of the samples after conditioning was registered, W_0, and then they were placed in a vacuum oven at 40 °C for 24 h to remove moisture. Afterward, the weight of the dried sample was registered, W_d. For the calculation of MC three samples per material were used and, MC was calculated with the following equation:

$$\mathrm{MC}\,(\%) = 100\% \times \frac{W_0 - W_d}{W_0} \tag{5}$$

2.5.9 Water solubility (WS). The samples used for the moisture content analysis were repurposed to study the water solubility of the sample, as they were already dried. The dried samples were submerged in approximately 5 mL of distilled water for 24 h at room temperature. Then, the water was removed carefully, and the films were dried in an oven at 110 °C for 24 h, and the final weight of the sample registered, W_f. The WS for each material tested was calculated with the following equation:

$$\mathrm{WS}\,(\%) = 100\% \times \frac{W_d - W_f}{W_d} \tag{6}$$

2.5.10 Water contact angle (WCA). Dataphysics OCA2000 (Charlotte, USA) instrument was used to measure the WCA. Samples were conditioned for 24 h in a conditioning room at 23 °C and 50% RH. The contact angle of sessile drops was measured after dosing a drop of 12 μL of ultrapure water (Merck Milli-Q). The image of the drop was captured after 10 s, to ensure the drop stabilization and maintain the same conditions between replicates. The WCA was measured at least 10 times per sample, and the results expressed as average ± SD.

2.5.11 Water vapor permeability (WVP). The water vapor permeability was tested using a TQC sheen (Capelle aan den IJssel, The Netherlands) permeability cup with an exposed surface area of 10 cm^2. The capsules were filled with 4 mL of water to simulate a 100% RH environment. The bioplastics were held using the seal ring of the permeability cup and secured with the cover ring. Then the capsule was placed inside a dry chamber with silica gel beads at 20% RH. Afterward, the weight loss of the capsules was registered periodically, plotted, and linearized. The slope of the resulting graph (g s^{-1}) was then divided by the surface area of 10 cm^2 (0.001 m^2) to calculate the water vapour transmission rate (WVTR). This value was later used to calculate the WVP using the following equation:

$$\mathrm{WVP} = \frac{\mathrm{WVTR} \times t}{P_{H_2O} \times \Delta\mathrm{RH}} \tag{7}$$

where t is the average thickness of the films, P_{H_2O} is the water vapour saturation pressure at the test temperature, and ΔRH is the difference in vapour pressure through the film. All samples were analysed by duplicate, and the results were expressed as average ± SD.

2.5.12 Antimicrobial properties. To determine the antimicrobial properties of the PL-grass bioplastic films, the growth inhibition of microorganisms on Mueller-Hinton Agar was measured in the presence of the tested films' disks. For this purpose, one-day cultures of *Escherichia coli* PBIO729 and *Staphylococcus aureus* PBIO901 were added to separate tubes

Open Access Article. Published on 27 March 2025. Downloaded on 11/8/2025 10:42:49 AM.
This article is licensed under a Creative Commons Attribution-NonCommercial 3.0 Unported Licence.

with sterile peptone water until they reached an optical density of 0.5 on the McFarland scale. The suspensions of microorganisms (200 μL each) were then applied to separate Petri dishes (90 mm in diameter) with Mueller–Hinton Agar, spread with disposable strokes and 2 disks of each film (9 mm in diameter) were applied. Discs with antibiotic meropenem (10 μg per disc), and PL (100 μg per disc) were used for comparison. After a 24 h incubation at 37 °C, the size of the inhibition zones was measured.[32]

Antimicrobial properties were also studied according to the ASTM E 2180-01 based on methodology described in previous study.[33] As the first step of the experiments, *E. coli* and *S. aureus*, cultures originated from 24 h growth (coming from stock cultures) were prepared. The concentrations of the cultures were standardized to 1.5×10^8 CFU mL^{-1}. The concentration of each culture was measured using Amersham Biosciences Ultraspec 10 Cell Density Meter (Slough, UK). The agar slurry was prepared by dissolving 0.9 g of NaCl and 0.3 g of agar–agar in 100 mL of deionized water and autoclaved for 15 min at 121 °C and equilibrated at 45 °C (one agar slurry was prepared for each strain). Then, 1 mL of the culture (separately) was placed into the 100 mL of agar slurry. The final concentration of each culture was 1.5×10^7 CFU mL^{-1} in molten agar slurry. The square samples of each film were introduced (separately) into the sterile Petri dishes with a diameter of 55 mm. Inoculated agar slurry (1.0 mL) was pipetted onto each square sample. The samples were incubated 24 h at 30 °C with relative humidity at 90%. After incubation the samples were aseptically removed from the Petri dishes and introduced into the 9 mL of sterile physiological saline (0.9% NaCl). The samples were then vortexed 1 min. The dispersion facilitated the complete release of the agar slurry from the samples. Then serial dilutions of the initial inoculum were performed. Each dilution was spread into the LB Agar (Carl Roth Gmbh) and incubated at 30 °C for 24 h. The results were presented as an average value with standard deviations.

2.5.13 Antioxidant activity. The antioxidant properties of the films were determined by examining the scavenging of ABTS radicals. For this purpose, 0.05 g samples were placed in 5 mL of distilled water, then incubated with shaking (200 rpm) for 1 h, and centrifuged (4000 rpm for 5 min) to obtain a clear extracts (supernatants) for further analyses.

ABTS radical scavenging activity was determined by mixing 30 μL of film extracts with 1500 μL of ABTS radical solution (produced by mixing 7 mM ABTS with 2.45 mM potassium persulfate) and incubating in the dark for 6 min. Then, the absorbance at 734 nm was measured using BMG Labtech Clariostar plus multiplate reader (Ortenberg, Germany). Trolox solutions were used to prepare the calibration curve. The results were expressed as μM Trolox equivalents (TE)/100 mg of film sample.

2.5.14 Life cycle assessment (LCA) and life cycle costing (LCC). The environmental impacts originating from the manufacturing of grass biomass bioplastic have been quantified according to the life cycle assessment (LCA) methodology following the ISO 14040/14044 standards.[34] The assessment was done considering a *cradle-to-gate* system boundary, which accounted for the raw material acquisition and their associated upstream processes, grass biomass bioplastic processing at the laboratory and the waste management of the generated side-streams. Primary data from our own experiments was utilized to construct the life cycle inventory (LCI), which is provided in the ESI Table S1† for the sake of transparency. A medium-voltage grid with 100% renewable energy (Switzerland mix) was considered for the modelling in the light of current accelerating decarbonisation of the European energy sector. The equipment depreciation is left aside. The life cycle impact assessment (LCIA) was carried out using OpenLCA 2.4 software and ecoinvent v3.11 database (released on November 19th, 2024). The life cycle impact assessment (LCIA) was carried out using the Environmental Footprint methodology recommended by the European Commission. For benchmark films, the following entries have been selected from the ecoinvent v3.11 database:

- Polylactic acid production, granulate|polylactic acid, granulate|Cutoff, U – GLO & extrusion, plastic film|extrusion, plastic film|Cutoff, U – RER.
- Polyethylene terephthalate production, granulate, bottle grade|polyethylene terephthalate, granulate, bottle grade|Cutoff, U – RER & extrusion, plastic film|extrusion, plastic film|Cutoff, U – RER.
- Packaging film production, low density polyethylene|packaging film, low density polyethylene|Cutoff, U – RER.

Besides, the OpenLCA 2.4 software and the ecoinvent v3.11 database has been utilized to determine the energy-related properties and cost aspects of conventional plastic materials. The cumulative energy demand (CED), cumulative exergy demand (CExD) and economic cost (based on a life cycle costing, LCC) of producing 1 kg of plastic film were calculated and compared with common plastic materials. For the grass bioplastic, the CED, CExD, and the economic cost are based on the material utilization for grass bioplastic, excluding capital expenses and the energy consumption to avoid biasing the results by high-energy consumption that is not representative of the full-scale process. However, this analysis can provide a useful overview on the potential cost of the developed material.

2.5.15 Statistical analysis. OriginLab2023b was used to perform the statistical analysis. Results were analysed by one-way analysis of variance (ANOVA) and Tukey's test was used to establish the significant differences between the samples with $p < 0.05$.

3. Results and discussion

3.1 Optimization of hydrolytic conditions during bioplastics preparation from grass

The content of the cellulose, hemicellulose, and lignin in the raw grass biomass was included in Table 2. Note that the sum of the reported values does not equal 100%., the rest corresponds to extractives and minerals (~11 wt%) whose compo-

Open Access Article. Published on 27 March 2025. Downloaded on 11/8/2025 10:42:49 AM.
This article is licensed under a Creative Commons Attribution-NonCommercial 3.0 Unported Licence.

Table 2 Cellulose, hemicellulose and lignin content in grass biomass compared with reported values in literature

Sample	Cellulose (wt%)	Hemicellulose (wt%)	Lignin (wt%)	Ref.
Brachiaria decumbens grass	50.3 ± 0.7	20.4 ± 0.5	18.2 ± 0.4	This work
Switchgrass	38.2 ± 0.7	28.3 ± 0.5	21.7 ± 1.0	30
Buffalo grass	~36.0	~29.0	~4.6	35
Bagasse	39.1 ± 0.7	27.3 ± 0.6	23.1 ± 0.9	30

sition has not been determined. The results indicate cellulose as the majoritarian component, followed by hemicellulose, in agreement with the values reported in the literature for other grass species.[30,35]

Grass-derived bioplastics obtained through alkaline hydrolysis (Fig. 1B and Fig. S1 in the ESI†) exhibited a uniform appearance, with a distinctive dark green colour and a paper-like texture. The films displayed a balanced combination of roughness and rigidity, which gradually decreased with increasing hydrolysis time, resulting in a smoother surface.

SEM micrographs of the bioplastics' cross-section (Fig. 1C and Fig. S2†) revealed the absence of large individual grass particles, confirming successful film formation after hydrolysis. The films exhibit a layered structure with visible fibrillar and sheet-like formations. Notably, as hydrolysis time increases, the layers become progressively more defined and compact, indicating structural rearrangement. This suggests that longer hydrolysis times enhance the cohesive structure and overall integrity of the films.

Fig. 1D shows the FTIR spectra of grass before and after hydrolysis, with G143 as a representative sample, highlighting the chemical changes induced by the process. Several characteristic peaks are observed in the grass prior to hydrolysis. The stretching vibration corresponding to hydroxyl groups, ν(O–H), appears at 3350 cm^{-1}, while the asymmetric, ν_{asym}(C–H), and symmetric, ν_{sym}(C–H), stretching vibrations, primarily associated with the methylene groups of the carbohydrate chain, are located at 2920 and 2850 cm^{-1}, respectively.[15] The band that appears in the range 1736–1729 cm^{-1} corresponds to the stretching of the carbonyl group (C═O), primarily due to the hemicellulose and lignin, typically related to ester groups.[36] The peaks between 1650 and 1500 cm^{-1} are mainly attributed to the aromatic stretching of C═C bonds, indicating the presence of lignin, and count also with the contribution of N–H bending of amines and amides in proteins and adsorbed water molecules. The region from 1460 cm^{-1} to 1316 cm^{-1}, shows multiple overlapping signals, including C–H in-plane bending, CH_2 asymmetric and symmetric bending, and O–H bending.[37] A minor band at 1250 cm^{-1} corresponds to C–O aryl groups present in lignin. Lastly, the strong signals at 1150 cm^{-1} and 1030 cm^{-1} correspond to C–O–C asymmetric stretching and C–O–C ring skeletal vibrations, due to the presence of hemicellulose and cellulose.[15,37]

Four notable changes are observed after hydrolysis. First, the band corresponding to the hydroxyl groups increases, as confirmed by the ratio of intensities between O–H band and C–H_2 band. Second, the C═O band at 1730 cm^{-1} shows a reduction in intensity, indicating that the alkaline hydrolysis produces the partial deacetylation of the hemicelluloses.[38] Third, the intensity of the C–O–C band at 1030 cm^{-1} also decreases, suggesting the breakdown of glycosidic bonds. Finally, the peaks centred at 1650 cm^{-1}, 1500 cm^{-1} and 1250 cm^{-1} due to the presence of aromatic compounds also increase intensity suggesting the possible formation of pseudo lignin.[39–41]

Fig. 1E illustrates the effect of NH_3 concentration at a fixed hydrolysis time (24 h) on the final chemical properties of the bioplastics. As NH_3 concentration increases, the intensity of the C–O–C linkage bands decreases, a trend also observed in films prepared at different times (Fig. S3†). This reduction is consistent with literature, indicating that the amorphous hemicellulose undergoes hydrolysis by breaking the C–O–C backbone and generating reducing sugars.[42] Using the C–H bond as a reference, the intensity of the O–H groups increases with the increase of NH_3 concentration. The ratio of intensities between these groups starts at 0.65 for NH_3 at 0.1 M, 24 h and increases up to 1.02 for NH_3 at 1M over the same period. This suggests that higher NH_3 concentrations lead to more extensive hydrolysis of the amorphous components.

To further investigate the impact of hydrolysis on the physicochemical properties of the developed bioplastics, we performed a thermogravimetric analysis. Fig. 2A illustrates the TGA curves showing the effect of time on grass hydrolysis at 1 M NH_3, while Fig. 2B presents the derivative curves for the same samples. Additional TGA curves for other films can be found in Fig. S4 in the ESI.† As shown in Fig. 2A and B, both raw grass and its derived bioplastics exhibit two main weight loss events. The first, around 100 °C, is attributed to the evaporation of water from the samples which corresponded to an approximately 5% weight loss for all the samples. The second weight loss, corresponds to the overlapped thermal degradation of the three primary components: cellulose (220 °C–360 °C),[37] hemicellulose (200–280 °C),[37] and lignin (290–700 °C).[37] Additionally, Fig. 2A indicates that G143 exhibits the lowest thermal stability, starting to degrade at lower temperatures compared to the grass and other samples. Moreover, the shoulder associated with hemicellulose degradation diminishes after hydrolysis, suggesting that hemicelluloses are particularly affected by the process, while cellulose remains relatively unaffected, at least for grass hydrolysis conducted at 8 and 24 hours. In contrast, grass bioplastics obtained after 43 hours of hydrolysis show also a decrease in the cellulose peak intensity, indicating partial hydrolysis of both hemicellulose and cellulose.

Regarding lignin, an increase in the intensity of the shoulder associated with its thermal degradation, centered at 400 °C, is observed after hydrolysis. This increase can be attributed to the condensation of sugars formed during hydrolysis, resulting in the formation of a pseudo-lignin.[41,43,44] This observation is further supported by the increase in aromatic groups detected in the FTIR analysis after hydrolysis.[41]

Open Access Article. Published on 27 March 2025. Downloaded on 11/8/2025 10:42:49 AM.
This article is licensed under a Creative Commons Attribution-NonCommercial 3.0 Unported Licence.

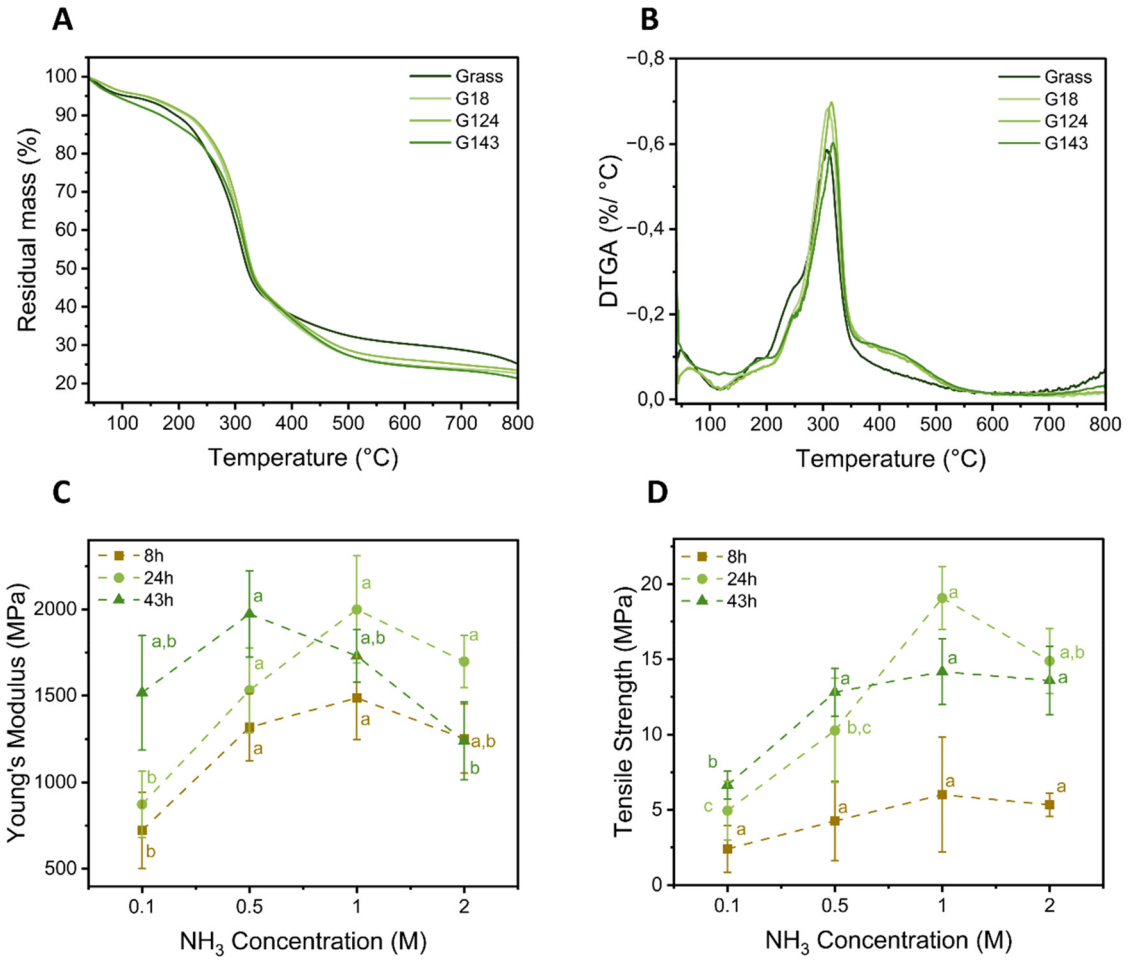

Fig. 2 Thermal and mechanical properties of grass-derived bioplastic films under varying hydrolysis conditions. (A) TGA of raw grass powder and bioplastic films obtained by hydrolysis using 1 M NH_3 and different hydrolytic times (8, 24, and 43 h); (B) derivative TGA curves (DTGA) of raw grass powder and bioplastic films obtained by hydrolysis using 1 M NH_3 and different hydrolytic times (8, 24, and 43 h); (C) Young's moduli (MPa) of grass bioplastic films after different alkaline hydrolysis conditions; (D) tensile strength (MPa) of grass bioplastic films after different alkaline hydrolytic conditions. Letters in plots (C) and (D) indicate whether samples are significantly different (different letters) or not (same letter) with a confidence level of 95%.

Lastly, to determine the optimal hydrolytic conditions for preparing bioplastics from grass biomass, we analysed the mechanical properties of the bioplastics, with key results presented in Fig. 2C and D.

Both reaction time and NH_3 concentration significantly impact the final mechanical properties of the bioplastics. The Young's modulus, which reflects the films' stiffness, remains low after a short hydrolysis time of 8 hours, indicating that the bioplastics have not yet developed sufficient structural integrity. This suggests that extended hydrolysis times are necessary to enhance the mechanical properties, regardless of the NH_3 concentration.

In terms of tensile strength, the films subjected to 8 hours of hydrolysis consistently display the lowest values, with no significant differences observed across varying NH_3 concentrations. However, hydrolysis times of 24 and 43 hours reduced the variation in both tensile strength and Young's modulus among the bioplastics. This indicates that longer hydrolysis not only improves the overall mechanical properties but also results in more uniform materials.

Maintaining a fixed hydrolysis time while increasing NH_3 concentration enhances both tensile strength and Young's modulus. This improvement arises from the increased hydrolysis of amorphous regions, which disrupts cell walls more effectively and facilitates the formation of a biocomposite material reinforced by cellulose fibrils. However, mechanical properties begin to decline beyond a critical NH_3 concentration. Excessive hydrolysis can lead to the degradation of amorphous components, resulting in a lower quality biocomposite. These results are in line with the results obtained by TGA. Notably, this critical NH_3 concentration varies with hydrolysis time: 1 M for 24 hours and 0.5 M for 43 hours.

Based on the mechanical test results, hydrolysis conditions of 1 M NH_3 for 24 hours were selected, as they produced rigid films with a Young's modulus of 1998 MPa ± 310 MPa and a tensile strength of 19 MPa ± 2 MPa. These conditions align

Open Access Article. Published on 27 March 2025. Downloaded on 11/8/2025 10:42:49 AM.
This article is licensed under a Creative Commons Attribution-NonCommercial 3.0 Unported Licence.

with those reported in the literature for the alkaline hydrolysis of other plant biomass.[24]

3.2 Optimizing conditions for preparation of antimicrobial bioplastics from grass biomass

PL was incorporated to optimize the functional properties of bioplastics from grass biomass. The bioplastics incorporating different PL concentrations exhibited a homogenous and smooth appearance, with no noticeable differences across varying PL content (Fig. 3A). However, significant differences were observed in the visual appearance of the films. The addition of PL resulted in a smoother surface with a subtle glow, enhancing the visual appeal. Moreover, the PL-containing samples lost their original paper-like rigidity and become ductile.

The SEM micrographs of the cross-sections (Fig. 3B) reveal significant structural changes with varying PL content. As previously discussed, the cross-section of G124 (0% PL) (shown in both Fig. 1B and 3B for comparison) is rough and fibrous, and presents loosely packed layers. Upon the addition of PL, the cross-sections become progressively more compact and denser. This structural densification suggests a strong interaction between the grass components and PL, leading to enhanced cohesion within the bioplastic matrix.[45]

To investigate the chemical interactions between grass polymer components and PL, the FTIR spectra of pure PL, G124 (0% PL), and GPL30 are compared in Fig. 3C. Spectra of other PL compositions are provided in Fig. S5 in ESI.†

The FTIR spectra of pure PL polymer shows a band at 3200 cm^{-1} corresponding to N–H stretching. A prominent signal at 3060 cm^{-1} accompanied by another at 1600cm^{-1} to 1500 cm^{-1} are attributed to the NH_3^+ side chain groups.[46,47] This is followed by distinct peaks at 2940 and 2860 cm^{-1}, which correspond to the asymmetric and symmetric stretching

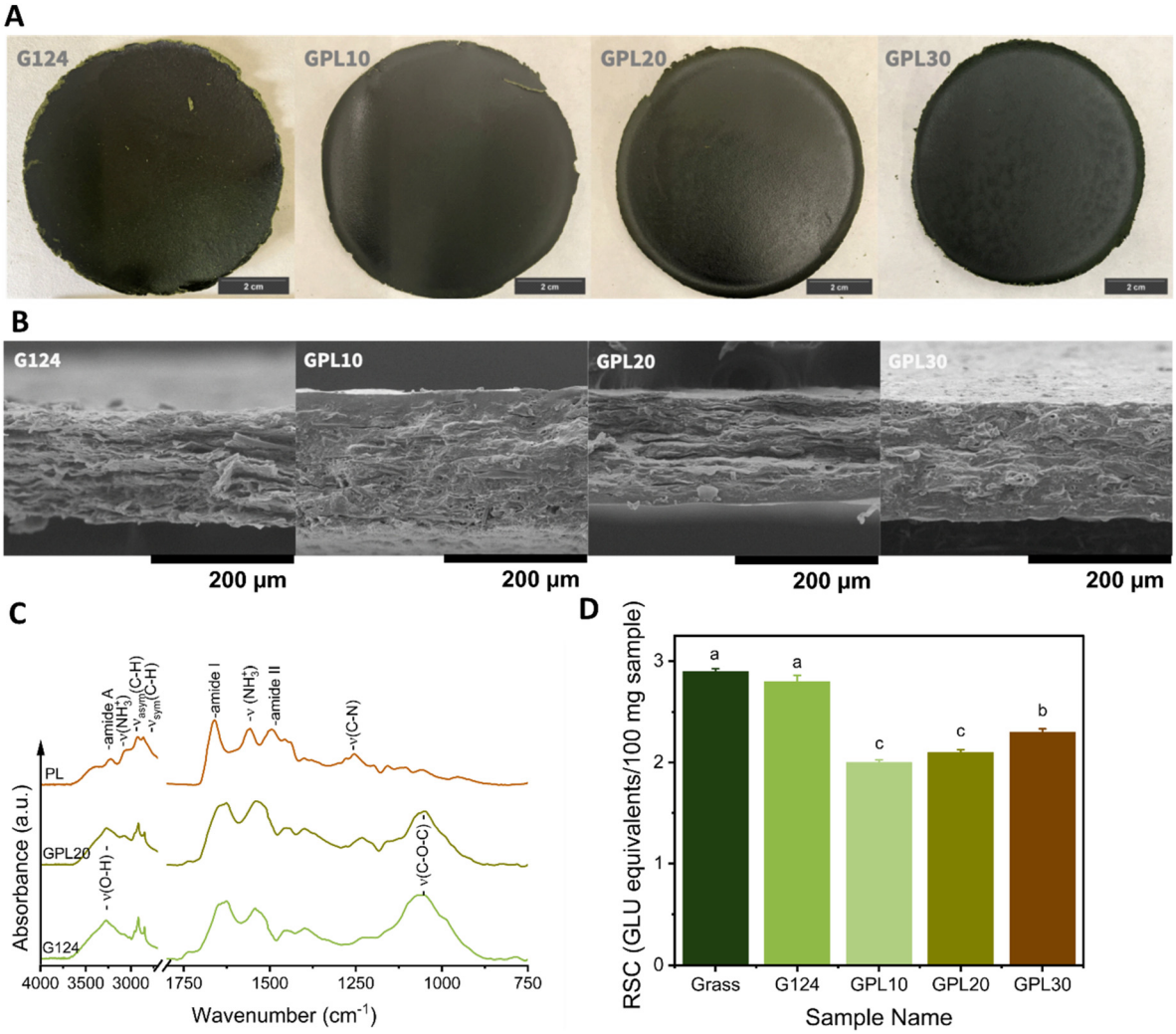

Fig. 3 Influence of ε-polylysine (PL) content on the structural and chemical properties of grass-derived bioplastic films. (A) Photographs depicting the visual appearance of bioplastic films produced with varying PL concentrations; (B) SEM micrographs illustrating the cross-sections of grass-PL bioplastics; (C) FTIR spectra comparing PL, hydrolyzed grass bioplastic without PL (G124), and grass-PL bioplastic with 20% PL content (GPL20); (D) reducing sugars content measured in the bioplastic films at different PL concentrations.

Open Access Article. Published on 27 March 2025. Downloaded on 11/8/2025 10:42:49 AM.
This article is licensed under a Creative Commons Attribution-NonCommercial 3.0 Unported Licence.

of C-H_2 bonds, respectively. The amide I band at 1640 cm^{-1} is characteristic of C═O stretching,[46,48] while the amide II band at 1530 cm^{-1} is due to the in-plane deformation of the NH group.[46] Lastly, the band at 1245 cm^{-1} corresponds to C–N stretching in the amide group.[48]

When comparing the FTIR spectra of pure PL, G124 (0% PL), and GPL30 (30%PL), no new peaks are observed in the GPL30 sample. This indicates that no covalent crosslinking occurs between the functional groups of the hydrolysed biomass and PL. However, shifts to lower wavenumbers are noted for bands corresponding to functional groups involved in hydrogen bonding, such as amide I and the C–N stretching. These shifts suggest that the interaction between PL and biomass is mainly due to hydrogen bonds.[49]

The formation of a Schiff base between the pending amino group of PL and the carbonyl groups of reducing sugars (produced during hydrolysis) was expected, which would have been indicated by the appearance of an imine peak around 1660 cm^{-1} in the FTIR spectra.[50] However, the absence of this peak suggests that PL did not react with the reducing sugars.[51] Schiff base formation would also have reduced the C═O band intensity due to the consumption of carbonyl groups.[50] Therefore, the reducing sugar content was measured in raw grass and bioplastics with varying PL content (0%, 10%, 20%, and 30% by weight) (Fig. 3D).

When comparing the reducing sugars content of raw grass with that of the bioplastics containing 0% PL, no significant increase in reducing sugars content was observed, which is unexpected since hydrolysis of polysaccharides yields reducing sugars.[42] However, as indicated by the earlier FTIR and TGA results, it is likely that the reducing sugars are reacting to form pseudo-lignin immediately after production, thereby preventing their interaction with the amino groups in PL. Additionally, an increase in PL content in the bioplastic formulations corresponds with a decrease in reducing sugar levels, likely due to the dilution effect of PL, which does not contribute to the final product's reducing sugars content.

The DTGA curves for selected samples are illustrated in Fig. 4A, while the complete DTGA curves for all samples can be found in ESI Fig. S6.† For PL, thermal degradation occurs in two distinct steps. The first degradation temperature, observed at 86 °C, primarily results from water evaporation, as PL is hygroscopic and rapidly absorbs moisture. Subsequently, thermal degradation is observed at two temperatures of maximum degradation rate: 297 °C and 444 °C. The first temperature is associated with transamidation reactions that reduce the molecular weight of the sample, leading to the formation of volatile compounds, while the second temperature is linked to the carbonization of the remaining components.[45]

Interestingly, the bioplastic films containing PL exhibit multiple degradation temperatures that do not correspond to those of the individual raw materials (PL and G124). These degradation steps present temperatures of maximum degradation rates at 190 °C and 210 °C, indicating the formation of specific interactions or complexes between PL and the polymers in the biomass, as well as with low molecular weight components present in the biomass.[50,52] A comparison with the literature and the FTIR spectra suggests that this stabilization may be attributed to hydrogen bonding between PL and the hydrolyzed grass components.[45,53]

To further investigate these interactions, DSC analysis was conducted to assess changes in the glass transition temperature (T_g) relative to PL content in the films. The DSC curves (Fig. 4B) reveal a single T_g within the studied temperature range. The addition of PL slightly decreases the T_g of the bioplastics, acting as a plasticizer. However, even with high concentrations of PL, the T_g only decreases by 2.7 °C compared to the film without PL. This minimal decrease in the glass transition temperature may be attributed to the hydrogen bonding that restricts the mobility of the polymer chains,[54] in addition

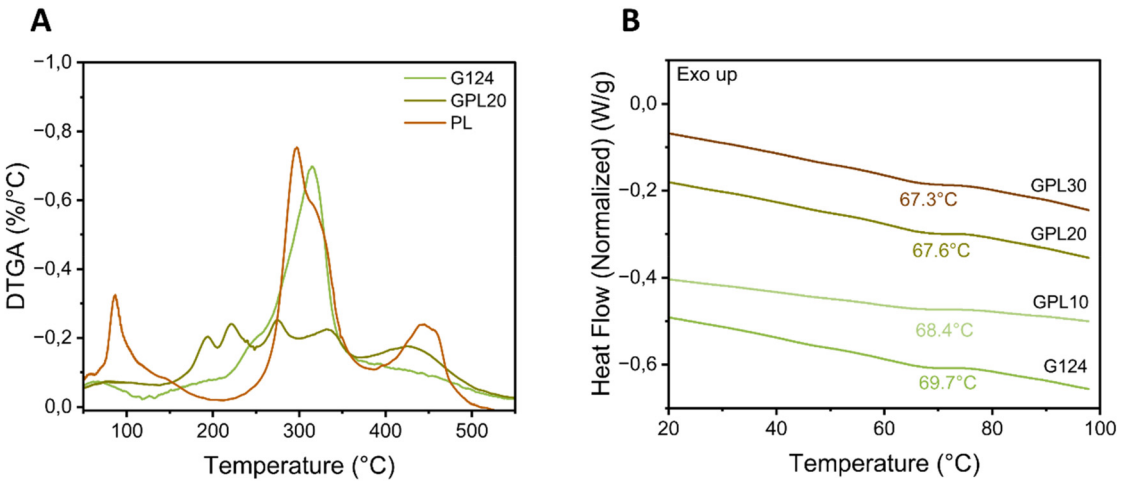

Fig. 4 Thermal analysis of grass-derived bioplastic films with PL. (A) DTGA curves of grass-derived bioplastic without PL, with 10% PL and PL alone; and (B) DSC heating curves of bioplastic films prepared from grass at different PL contents.

Open Access Article. Published on 27 March 2025. Downloaded on 11/8/2025 10:42:49 AM.
This article is licensed under a Creative Commons Attribution-NonCommercial 3.0 Unported Licence.

Table 3 Mechanical properties, cumulative energy demand (CED), cumulative exergy demand (CExD) and economic cost (based on a life cycle costing, LCC) of the grass-derived bioplastics with PL and its comparison with bioplastics developed in the literature and polymers used in the packaging industry

Material	Young's modulus (MPa)	Tensile strength (MPa)	Strain at break (%)	Cumulative energy demand (CED)	Cumulative exergy demand (CExD)	Cost of production (EUR per kg)	Ref.
G124	2055 ± 126	21 ± 1	1.1 ± 0.1	—	—	—	This work
GPL10	846 ± 91	12 ± 3	1.8 ± 0.4	25.4 MJ	26.4 MJ	—	This work
GPL20	735 ± 119	10 ± 1	1.6 ± 0.2			34.1 (1.41 EUR per kg with no ε-polylysine)	This work
GPL30	583 ± 88	10 ± 1	2.75 ± 0.3				This work
LDPE	100–300	9–15	300–500	99.7 MJ	115.9 MJ	2.97	55 and 56
HDPE	800–1600	10–60	150–400				57 and 58
Poly-lactic acid (PLA)	8600	120	30	77.5 MJ	99.7 MJ	1.48	64
Thermoplastic starch	400–1000	0.9–22	3–60	67.8 MJ	78.8 MJ	0.45	59
Lime peel	441 ± 43	14 ± 2	4.6 ± 1.2	—	—	—	61
Avocado peel	342 ± 46	18 ± 3	16.8 ± 6.1	—	—	—	62
Potato peel	432 ± 86	13 ± 2	18.4 ± 4.3	—	—	—	63

to the higher molecular weight of PL compared to other common plasticizers, such as glycerol.

Subsequently, we analyzed the mechanical properties of the bioplastics, with the results summarized in Table 3. The data indicate that PL effectively acted as a plasticizer within the bioplastic matrix, as confirmed by the DSC analysis.[49] Notably, the addition of PL significantly reduced the Young's modulus from approximately 2000 MPa to around 750 MPa with 20% PL incorporation. Furthermore, the inclusion of PL enhanced the ductility of the material, as evidenced by the increase in strain at break, which rose from 1.1% to 1.6% (Table 3). However, the tensile strength of the grass bioplastics decreased with the addition of PL, dropping from 21 MPa at 0% PL to 10 MPa.

When comparing the properties of the synthesized bioplastics with those of conventional packaging materials (Table 3), it is evident that the Youngs modulus and tensile strength (TS) of these bioplastics are comparable to those of commonly used packaging materials such as low-density polyethylene (LDPE),[55,56] high-density polyethylene (HDPE),[57,58] and thermoplastic starch.[59] However, the ductility of the PL-grass films is noticeably lower than that of these materials, which could limit their applicability in scenarios where ductility is crucial. Considering their high elastic modulus and tensile strength, these bioplastics may be well-suited for rigid packaging applications, such as trays or covers, as illustrated in the graphical abstract.[60]

In comparison to lime peel,[61] avocado peel[62] and potato peel[63] derived bioplastics the rigidity of the PL-grass biofilms is nearly doubled, while the tensile strength falls within a similar range. However, the previous bioplastics have demonstrated superior ductility.

In addition, Table 3 presents the sustainability assessment of the grass-derived bioplastics, focusing on their cumulative energy demand (CED), cumulative exergy demand (CExD), and economic cost based on life cycle costing (LCC). The results underscore the potential advantages of these bioplastics over conventional plastics. The CED and CExD of the bioplastic containing 20% PL (GPL20) were determined at 25.4 MJ and 26.4 MJ, respectively, which are substantially lower than those of widely used LDPE (99.7 MJ, 115.9 MJ) and PLA (77.5 MJ, 99.7 MJ), indicating a reduced environmental footprint in terms of energy consumption. However, the economic analysis highlights that the production cost of GPL20 remains relatively high, primarily due to the inclusion of PL. Notably, when excluding PL from the cost calculation, the price (1.41 EUR per kg) becomes competitive with PLA (1.48 EUR per kg). Future advancements in PL production and cost optimization could further improve the economic feasibility of these bioplastics. Given their lower energy demands and the potential for future cost reductions, these materials show promise as sustainable alternatives for rigid packaging applications, aligning with circular economy principles in the packaging industry.

Regarding interactions with water, the addition of PL yields notable changes. As shown in Fig. 5A, the moisture content of the samples is significantly reduced with the incorporation of PL. This effect may be attributed to the formation of hydrogen bonds, where the hydroxyl groups in the grass interact with PL, thereby limiting moisture absorption and enhancing the structural integrity of the bioplastic.[65]

As illustrated in Fig. 5B, the solubility of the samples initially decreases by 50% with the addition of up to 20 wt% of PL. However, as the PL content increases beyond this point, the solubility subsequently rises, with PL alone exhibiting 100% solubility in water. Notably, the GPL10 and GPL20 samples demonstrate the best water stability, showing significant resistance to solubility compared to the sample without PL (G124).

The water vapor permeability results are summarized in Fig. 5C. The addition of PL to the bioplastic films increases the WVP; however, no statistically significant differences were observed with respect to varying PL content. The values obtained are comparable to those reported in the literature for other bioplastics, like mango peel,[66] wheat starch[67] and potato starch films,[68] with WVP values of 8.8×10^{-9}, 2.8×10^{-9} and 1.5×10^{-9} g Pa^{-1} s^{-1} m^{-1}, respectively.

Finally, the results of the water contact angle analysis support the role of hydrogen bonding as a stabilizing force in

Open Access Article. Published on 27 March 2025. Downloaded on 11/8/2025 10:42:49 AM.
This article is licensed under a Creative Commons Attribution-NonCommercial 3.0 Unported Licence.

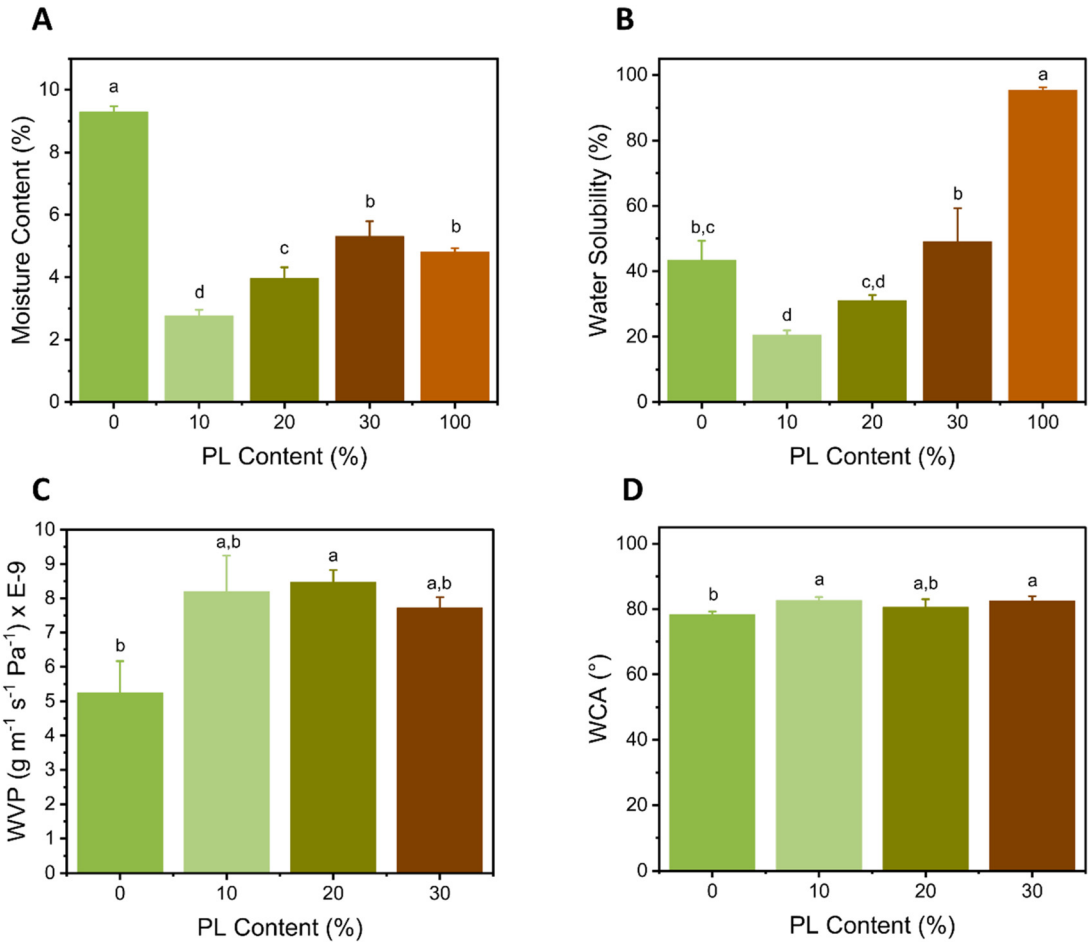

Fig. 5 Water interaction of biofilms containing PL. (A) Moisture content (%), (B) water solubility (%), (C) water vapour permeability (g m^{-1} s^{-1} Pa^{-1}), D. Water contact angle (°). Letters in plots indicate whether samples are significantly different (different letters) or not (same letter) with a confidence level of 95%.

the PL-grass films. As illustrated in Fig. 5D, the incorporation of PL renders the films slightly more hydrophobic. This change arises from the hydrogen bonding between the polar groups of the components, which reduces the likelihood of water molecules interacting with the film.[69]

Finally, the antimicrobial properties of bioplastics were studied against both Gram-negative (*E. coli*) and Gram-positive (*S. aureus*) bacteria. The results obtained using the ASTM E 2180-01 method, shown in Fig. 6A, demonstrate that the growth of both bacteria is inhibited in the presence of PL. For *E. coli*, no bacterial growth was observed after the addition of 20% PL, while for *S. aureus*, growth inhibition occurred only at 30% PL.

To confirm the diffusion of PL, an agar diffusion test was performed with the film against *S. aureus* (Fig. S7†) and *E. coli* (Fig. S8†). The results indicate that bioplastics acquire antimicrobial properties with the addition of PL.[25,26] A clear increase in the inhibition halo is observed as PL content increases, while the film containing 0% PL (G124) does not generate an inhibition halo. In contrast, PL control discs show a distinct inhibition halo, confirming its role as an antimicrobial agent.

The inhibition mechanisms of PL against Gram-positive and Gram-negative bacteria have been extensively reported. PL inhibits bacterial growth by affecting the permeability of their cell walls and membranes.[25] For *E. coli*, it has been shown that PL interacts with the phospholipid groups in the cell membrane, causing distortion and damage.[25] In the case of *S. aureus*, PL induces structural changes in the peptidoglycans of the cell wall, increasing permeability.[70]

Regarding the antioxidant properties of the film an interesting behaviour can be observed in Fig. 6B. The antioxidants that quench and scavenge the radicals of ABTS are compounds capable of donating hydrogen or electrons, additionally the antioxidant compounds are responsible of stabilizing the new radical generated within the structure. Phenols have shown to produce this antioxidant behaviour, that are strongly affected by the degree of substitution of the aromatic ring.[71] This explains the different behaviour observed for the bioplastic films. Firstly, when no PL is present in the films, the anti-

Open Access Article. Published on 27 March 2025. Downloaded on 11/8/2025 10:42:49 AM.
This article is licensed under a Creative Commons Attribution-NonCommercial 3.0 Unported Licence.

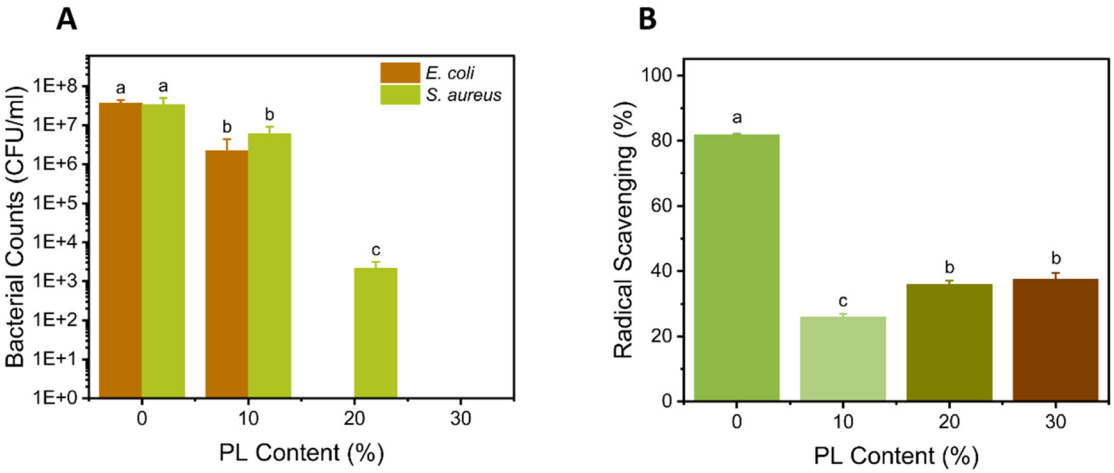

Fig. 6 Antimicrobial and antioxidant properties for grass-PL-derived bioplastics. (A) ASTM E 2018-01 antimicrobial results for bioplastics containing different content of PL against *E. Coli* and *S. aureus*, (B) ABTS antioxidant assay results for bioplastics containing different content of PL. Letters in plots indicate whether samples are significantly different (different letters) or not (same letter) with a confidence level of 95%.

oxidant properties are solely dependent on the hydrolysis products of the grass. The alkaline hydrolysis of the grass produces phenols, through lignin hydrolysis, and reducing sugars, through hemicelluloses hydrolysis.[42] Both compounds can stabilize and scavenge the radicals of ABTS effectively reaching a scavenging percentage of up to 80%. However, a different behaviour is observed after the incorporation of PL. With the addition of PL the availability of this antioxidants is reduced due to a diluting effect generated by the PL. With the addition of PL, the hydrogen bonds between PL and hydrolysis products decreases significantly the scavenging capacity (25%). This is due to the inability of the highly antioxidant compounds of hydrolysis to donate hydrogen atoms to stabilize the radicals as they are imprisoned by the interaction with PL. At last, the increase in PL to higher percentages also lead to an increase in scavenging percentage that can be attributed to the increase of amino groups in lysine, which concentration increases as more PL is present in the film. This amino groups have been reported to have a low antioxidant activity[72].

Life cycle assessment (LCA) was applied to grass biomass bioplastic development to explore its potential for sustainable material development. The disaggregated climate change potential for a 100 year time horizon (expressed in CO_2 equivalents) of the GPL20 film for a *cradle-to-gate* system boundary is provided in Fig. 7. The production of the GPL20 film has a footprint of 3.29 kg CO_2 equiv. kg^{-1}, where steps 2, and specially steps 5 and 6, bear the largest share. Spherically, the step 2 (drying) has a contribution of 0.46 kg CO_2 equiv. kg^{-1}, while steps 5 and 6 add 1.78 and 1.01 kg CO_2 equiv. kg^{-1}, respectively. The largest contributors to greenhouse gas emissions during steps 5 are the use of ammonia (0.89 kg CO_2 equiv. kg^{-1}), the electricity consumption (0.63 kg CO_2 equiv. kg^{-1}) and the incorporation of ε-polylysine (0.25 kg CO_2 equiv. kg^{-1}). It is important to note that the *climate change potential* of the GPL20 films remains below the footprint showed by benchmark plastic films such as PLA (3.45 kg CO_2 equiv. kg^{-1}), PET (3.62 kg CO_2 equiv. kg^{-1}), LDPE (3.40 kg CO_2 equiv. kg^{-1}). Similarly, the grass bioplastics show a lower carbon footprint than the 4.4–4.8 kg CO_2 equiv. kg^{-1} reported for pomegranate peel extract-infused carboxymethyl cellulose films (that have antioxidant and antibacterial properties),[73] while it remains at the lower end of the range of 1.82–6.00 kg CO_2 equiv. kg^{-1} showed by alveolus trays produced by thermoforming of vegetable waste.[74] More importantly, if the biogenic carbon content is accounted as sequestered carbon according to the PAS 2050 carbon accounting protocol (*i.e.*, long-term applications),[75,76] a total *climate change potential* of 1.69 kg CO_2 equiv. kg^{-1} is achieved. The reduced carbon footprint over petroleum-derived plastic films matches literature and highlights the potential of bio-based products to deliver materials with reduced greenhouse gas emissions.[77]

Additional environmental impact categories in the light of the EF v3.1 impact assessment methodology are provided in Fig. S9.† The results show a remarkable variability depending on the category under consideration. With values of 36 MJ kg^{-1}, 1.08×10^{-4} kg Sb eq. kg^{-1}, and 0.25 kBq U235 eq. kg^{-1}, significant benefits are observed in categories such as energy resources (non-renewable), material resources (metals and minerals) and ionizing radiation (human health), respectively. These benefits are explained by the biobased character of the grass bioplastics, which avoids the need to extract non-renewable resources. On the contrary, the acidification and water use derived from grass biomass bioplastic manufacturing results one-to-two orders of magnitude larger than that observed for conventional packaging plastics. 99% of the acidification originates from the NH_3 gas released during solvent evaporation (step 6),[78] while 78% of water uses are related to the significant electricity consumption during steps 5 and 6. Therefore, implementing an ammonia recovery process and enhanced process efficiency upon upscaling can certainly

Open Access Article. Published on 27 March 2025. Downloaded on 11/8/2025 10:42:49 AM.
This article is licensed under a Creative Commons Attribution-NonCommercial 3.0 Unported Licence.

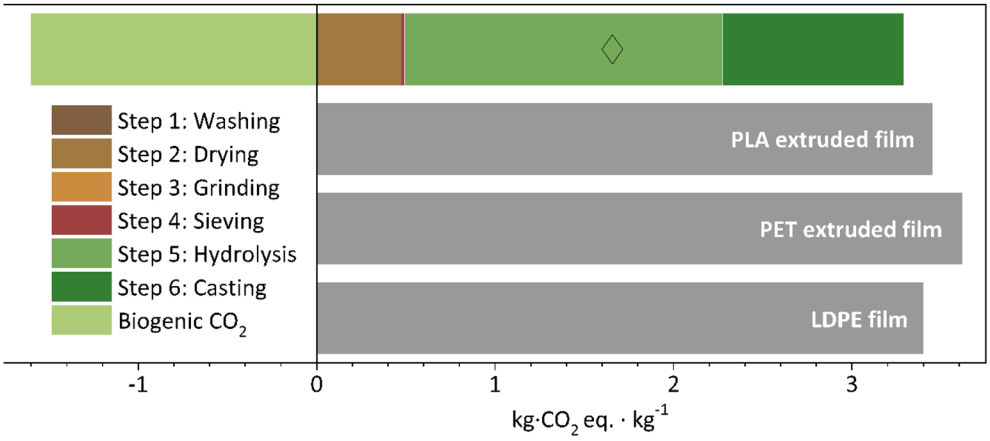

Fig. 7 Disaggregated climate change potential for "grass bioplastic" fabrication (*cradle-to-gate* system boundary). The diamond represents the total impact considering credits for biogenic carbon uptake. The climate change potential of benchmark packaging plastic films is provided for comparison.

reduce the environmental impacts and increase the sustainability of the grass bioplastic. In the light of LCA results, the developed materials show promising attributes for sustainable packaging solutions.

4. Conclusions

Bioplastics were successfully prepared from grass biomass, which underwent alkaline hydrolysis with NH_3. The resulting films exhibited competitive mechanical properties against petroleum-derived plastics, achieving a Young's modulus of 2200 MPa and a tensile strength of 22 MPa. However, these films demonstrated low ductility, with a strain at break of less than 1%. The mechanical properties were influenced by both the hydrolysis time and the concentration of the NH_3 solution used. Optimal conditions were established at 24 hours of hydrolysis with 1 M NH_3, yielding the best mechanical performance. TGA and FTIR analyses confirmed that the hydrolysis process preferentially targeted hemicellulose and lignin polymers. Although these techniques provide useful insights into compositional changes, direct polymer molecular weight measurements would better elucidate chain scission and reorganization during hydrolysis, which represents a promising avenue for future research.

To enhance the properties of the bioplastics and incorporate antimicrobial functionality, grass biomass was combined with the antimicrobial PL peptide. The primary interaction between PL and hydrolyzed grass was identified as hydrogen bonding, as evidenced by FTIR spectra. Notably, there was no chemical crosslinking between PL and the hydrolysis products. Instead, the reducing sugars are believed to form pseudo-lignin rather than crosslinking with PL, as indicated by TGA, RSC, and FTIR results.

The inclusion of PL in the hydrolysis mixture produced of more flexible materials due to its plasticizing effect, resulting in reduced Young's modulus and tensile strength while slightly enhancing ductility. This effect was further confirmed by a decrease in the glass transition temperature (T_g) with increasing PL content, and the films' cross-sectional morphology became smoother compared to bioplastics without PL.

In terms of water interactions, all bioplastics maintained a moisture content below 10%. The addition of up to 20 wt% PL resulted in a significant reduction in water solubility. These observations were attributed to hydrogen bonding interactions between the polar groups of the hydrolyzed biomass and PL, inhibiting water absorption.

Moreover, the incorporation of PL into the bioplastics resulted in antimicrobial films effective against *E. coli* and *S. aureus*. The GPL20 films demonstrated complete inhibition of *E. coli* growth and a 99% reduction in *S. aureus* growth compared to films lacking PL. Furthermore, antioxidant properties were observed, which can be beneficial for extending food shelf life.

Life cycle assessment highlights the potential of grass biomass for sustainable material development, outperforming benchmark packaging biobased or fossil-based alternatives. The ease of processing in combination with the biogenic carbon storage results in films with a *cradle-to-gate* climate change potential of 1.69 kg CO_2 eq. kg^{-1}, while PLA, PET and LDPE films carbon footprint values of 3.40–3.62 kg CO_2 eq. kg^{-1}.

Given their antimicrobial properties, favourable mechanical characteristics, and interactions with water, GPL20 films represent a promising material for further investigation into sustainable food packaging applications, particularly for rigid or single-use packaging solutions. However, it is important to note that this study was conducted on a laboratory scale (3 g batches) sufficient for prototyping, such as fabricating a sample tray. Future work should focus on scaling up production by optimizing drying techniques, improving biomass dispersion, and evaluating large-scale manufacturability to facilitate industrial adoption.

 This journal is © The Royal Society of Chemistry 2025

Open Access Article. Published on 27 March 2025. Downloaded on 11/8/2025 10:42:49 AM.
This article is licensed under a Creative Commons Attribution-NonCommercial 3.0 Unported Licence.

Data availability

The data supporting this article have been included as part of the ESI.†

Conflicts of interest

The authors declare that they have no known competing financial interests or personal relationships that could have appeared to influence the work reported in this paper.

Acknowledgements

J. D. E. S. would like to thank the members of the Sustainable Biocomposite Materials (SusBioComp) group for their support and advice during the seminar sessions. Gratitude is also extended to the members of Sardon's Lab for their assistance during their time in the laboratory. Additionally, thanks are given to Jorge Olmedo for conducting the TGA analysis. E. L. is grateful for the financial support from the University of the Basque Country (Convocatoria de ayudas a grupos de investigación GIU21/010). D. M. gratefully acknowledges financial support from the Basque Science Foundation for Science (Ikerbasque), POLYMAT, the University of the Basque Country (UPV/EHU), and the European Union's Horizon Europe research and innovation programme under the Marie Skłodowska-Curie grant agreement No. 101103474. Additionally, D. M. thanks the support from the María de Maeztu Excellence Unit (CEX2023-001303-M), funded by MCIN/AEI/10.13039/501100011033.

References

1 Plastics Europe, 2023.
2 Y. Chen, A. K. Awasthi, F. Wei, Q. Tan and J. Li, *Sci. Total Environ.*, 2021, **752**, 141772.
3 S. Alavi, S. Thomas, K. P. Sandeep, N. Kalarikkal, J. Varghese and S. Yaragalla, *Polymers for Packaging Applications*, CRC Press, 2014.
4 B. Tajeddin and M. Arabkhedri, in *Polymer Science and Innovative Applications*, ed. M. A. A. AlMaadeed, D. Ponnamma and M. A. Carignano, Elsevier, 2020, pp. 525–543.
5 J. Tan, S. K. Tiwari and S. Ramakrishna, *Mater. Circ. Econ.*, 2021, **3**, 7.
6 K. Babaremu, O. P. Oladijo and E. Akinlabi, *Adv. Ind. Eng. Polym. Res.*, 2023, **6**, 333–340.
7 Plastics Europe, 2022.
8 A. Kumar, S. Mishra, R. Pandey, Z. G. Yu, M. Kumar, K. S. Khoo, T. K. Thakur and P. L. Show, *TrAC Trends Anal. Chem.*, 2023, **158**, 116869.
9 Z. Li, Y. Yang, X. Chen, Y. He, N. Bolan, J. Rinklebe, S. S. Lam, W. Peng and C. Sonne, *Chemosphere*, 2023, **313**, 137637.
10 E. C. Emenike, C. J. Okorie, T. Ojeyemi, A. Egbemhenghe, K. O. Iwuozor, O. D. Saliu, H. K. Okoro and A. G. Adeniyi, *Heliyon*, 2023, **9**, e20440.
11 L. He, Z. Li, Q. Jia and Z. Xu, *Science*, 2023, **379**, 547–547.
12 Z. Qaiser, M. Aqeel, W. Sarfraz, Z. Fatima Rizvi, A. Noman, S. Naeem and N. Khalid, *Case Stud. Chem. Environ. Eng.*, 2023, **8**, 100536.
13 D. G. Bucknall, *Philos. Trans. R. Soc., A*, 2020, **378**, 20190268.
14 K. N. Onwukamike, S. Grelier, E. Grau, H. Cramail and M. A. R. Meier, *ACS Sustainable Chem. Eng.*, 2019, **7**, 1826–1840.
15 A. I. Quilez-Molina, U. Chandra Paul, D. Merino and A. Athanassiou, *ACS Sustainable Chem. Eng.*, 2022, **10**, 15402–15413.
16 A. N. M. A. Haque, R. Remadevi, X. Wang and M. Naebe, *Mater. Chem. Phys.*, 2020, **239**, 122009.
17 J. S. Yaradoddi, N. R. Banapurmath, S. V. Ganachari, M. E. M. Soudagar, A. M. Sajjan, S. Kamat, M. A. Mujtaba, A. S. Shettar, A. E. Anqi, M. R. Safaei, A. Elfasakhany, M. I. Haque Siddiqui and M. A. Ali, *J. Mater. Res. Technol.*, 2022, **17**, 3186–3197.
18 D. Merino, R. Simonutti, G. Perotto and A. Athanassiou, *Green Chem.*, 2021, **23**, 5956–5971.
19 D. Merino and A. Athanassiou, *Chem. Eng. J.*, 2023, **454**, 140171.
20 L. Chen, T. Bi, E. Lizundia, A. Liu, L. Qi, Y. Ma, J. Huang, Z. Lu, L. Yu, H. Deng and C. Chen, *Innovation*, 2024, **5**, 100655.
21 Z. Hao, W. Y. Hamad and P. Yaseneva, *Chem. Eng. J.*, 2023, 147160.
22 R. L. de Lapuente Díaz de Otazu, O. Akizu-Gardoki, B. de Ulibarri, M. Iturriondobeitia, R. Minguez and E. Lizundia, *Sustain. Prod. Consum.*, 2021, **29**, 718–729.
23 M. F. de Souza, Ç. Akyol, B. Willems, A. Huizinga, S. van Calker, M. Van Dael, A. De Meyer, R. Guisson, E. Michels and E. Meers, *Waste Manage.*, 2024, **182**, 1–10.
24 J. C. García, A. Alfaro, J. M. Loaiza, S. Lozano-Calvo and F. López, *Biomass Convers. Biorefin.*, 2024, **14**, 8307–8320.
25 L. Wang, C. Zhang, J. Zhang, Z. Rao, X. Xu, Z. Mao and X. Chen, *Front. Bioeng. Biotechnol.*, 2021, **9**, 748976.
26 S. Chen, S. Huang, Y. Li and C. Zhou, *Front. Chem.*, 2021, **9**, 659304.
27 K. Ushimaru, Y. Hamano, T. Morita and T. Fukuoka, *ACS Omega*, 2019, **4**, 9756–9762.
28 K. Ushimaru, T. Morita and T. Fukuoka, *ACS Omega*, 2020, **5**, 22793–22799.
29 A. Álvarez, S. Cachero, C. González-Sánchez, J. Montejo-Bernardo, C. Pizarro and J. L. Bueno, *Carbohydr. Polym.*, 2018, **189**, 250–256.
30 M. Ioelovich, *Bioresources*, 2015, **10**(1), 1879–1914.
31 Ł. Łopusiewicz, N. Śmietana, D. Paradowska and E. Drozłowska, *Microorganisms*, 2022, **10**, 300.
32 S. Macieja, B. Środa, B. Zielińska, S. Roy, A. Bartkowiak and Ł. Łopusiewicz, *Int. J. Mol. Sci.*, 2022, **23**, 15560.

Open Access Article. Published on 27 March 2025. Downloaded on 11/8/2025 10:42:49 AM.
This article is licensed under a Creative Commons Attribution-NonCommercial 3.0 Unported Licence.

33 Ł. Łopusiewicz, P. Kwiatkowski, E. Drozłowska, P. Trocer, M. Kostek, M. Śliwiński, M. Polak-Śliwińska, E. Kowalczyk and M. Sienkiewicz, *Polymers*, 2021, **13**, 499.
34 A. Laurent, B. P. Weidema, J. Bare, X. Liao, D. Maia de Souza, M. Pizzol, S. Sala, H. Schreiber, N. Thonemann and F. Verones, *J. Ind. Ecol.*, 2020, **24**, 986–1003.
35 C. Chan, D. Martin, E. Gauthier, P. Jensen, B. Laycock and S. Pratt, *Polymers*, 2022, **14**, 3704.
36 V. E. Ottah, A. L. Ezugwu, T. C. Ezike and F. C. Chilaka, *Heliyon*, 2022, **8**, e09714.
37 G. S. Cano-Díaz, A. Rosas-Aburto, E. Vivaldo-Lima, L. Flores-Santos, M. A. Vega-Hernández, M. G. Hernández-Luna and A. Martinez, *Ind. Eng. Chem. Res.*, 2021, **60**, 3502–3515.
38 W. Peng, L. Wang, M. A. K. O. T. O. Ohkoshi and M. Zhang, *Cellul. Chem. Technol.*, 2015, **49**(9–10), 756–764.
39 D. M. D. Carvalho and J. L. Colodette, *BioResources*, 2017, **12**, 6907–6923.
40 R. Kumar, F. Hu, P. Sannigrahi, S. Jung, A. J. Ragauskas and C. E. Wyman, *Biotechnol. Bioeng.*, 2013, **110**, 737–753.
41 S. D. Shinde, X. Meng, R. Kumar and A. J. Ragauskas, *Green Chem.*, 2018, **20**, 2192–2205.
42 S. Park, S. J. Kim, K. C. Oh, L. Cho, Y. K. Jeon and D. H. Kim, *Energy*, 2023, **283**, 128548.
43 M. Henrikki Sipponen, V. Pihlajaniemi, S. Sipponen, O. Pastinen and S. Laakso, *RSC Adv.*, 2014, **4**, 23177–23184.
44 P. Sannigrahi, D. H. Kim, S. Jung and A. Ragauskas, *Energy Environ. Sci.*, 2011, **4**, 1306–1310.
45 S. Razani and A. Dadkhah Tehrani, *Polym. Bull.*, 2024, **81**, 4893–4909.
46 M. Rozenberg and G. Shoham, *Biophys. Chem.*, 2007, **125**, 166–171.
47 D. Sebben and P. Pendleton, *Spectrochim. Acta, Part A*, 2014, **132**, 706–712.
48 G. Zhu, N. Guo, X. Yan, J. Dong, X. Chen and H. Lu, *Coatings*, 2023, **13**, 1832.
49 Z. Yu, G. Rao, Y. Wei, J. Yu, S. Wu and Y. Fang, *Int. J. Biol. Macromol.*, 2019, **141**, 545–552.
50 X. He, Y. Li, L. Zhang, R. Du, Y. Dai and Z. Tan, *Cellulose*, 2021, **28**, 2833–2847.
51 S. C. Shukla, A. Singh, A. K. Pandey and A. Mishra, *Biochem. Eng. J.*, 2012, **65**, 70–81.
52 W. Liao, X. Liu, Q. Zhao, Z. Lu, A. Feng and X. Sun, *Int. J. Biol. Macromol.*, 2023, **253**, 127231.
53 J. Hu, W. Jiao, Q. Chen, B. Liu and M. Fu, *Food Sci. Nutr.*, 2023, **11**, 5188–5198.
54 R. G. M. van der Sman, *J. Phys. Chem. B*, 2013, **117**, 16303–16313.
55 G. Wypych, in *Handbook of Polymers (Second Edition)*, ed. G. Wypych, ChemTec Publishing, 2016, pp. 178–184.
56 X. Zhao, K. Cornish and Y. Vodovotz, *Environ. Sci. Technol.*, 2020, **54**, 4712–4732.
57 G. Wypych, in *Handbook of Polymers (Second Edition)*, ed. G. Wypych, ChemTec Publishing, 2016, pp. 156–163.
58 M. Zhang, G. M. Biesold, W. Choi, J. Yu, Y. Deng, C. Silvestre and Z. Lin, *Mater. Today*, 2022, **53**, 134–161.
59 Y. Zhang, C. Rempel and Q. Liu, *Crit. Rev. Food Sci. Nutr.*, 2014, **54**, 1353–1370.
60 V. Dwibedi, G. Kaur, N. George, P. Rana, Y. Ge and T. Sun, *Food Packag. Shelf Life*, 2024, **46**, 101385.
61 P. Rodsamran and R. Sothornvit, *Food Hydrocolloids*, 2019, **97**, 105173.
62 D. Merino, L. Bertolacci, U. C. Paul, R. Simonutti and A. Athanassiou, *ACS Appl. Mater. Interfaces*, 2021, **13**, 38688–38699.
63 D. Merino, U. C. Paul and A. Athanassiou, *Food Packag. Shelf Life*, 2021, **29**, 100707.
64 N. G. Khouri, J. O. Bahú, C. Blanco-Llamero, P. Severino, V. O. C. Concha and E. B. Souto, *J. Mol. Struct.*, 2024, **1309**, 138243.
65 G. Wypych, *Handbook of Material Weathering*, Elsevier, 2018.
66 C. Torres-León, A. A. Vicente, M. L. Flores-López, R. Rojas, L. Serna-Cock, O. B. Alvarez-Pérez and C. N. Aguilar, *LWT*, 2018, **97**, 624–631.
67 G. P. Bruni, J. P. de Oliveira, L. M. Fonseca, F. T. da Silva, A. R. G. Dias and E. da Rosa Zavareze, *Starch*, 2020, **72**, 1900051.
68 A. Rejak, A. Wójtowicz, T. Oniszczuk, D. Niemczuk and M. Nowacka, *Teka Komisji Motoryzacji i Energetyki Rolnictwa*, 2014, **14**(3), 89–94.
69 Q. Sun, *Molecules*, 2022, **27**, 7009.
70 Z. Tan, Y. Shi, B. Xing, Y. Hou, J. Cui and S. Jia, *Bioresour. Bioprocess.*, 2019, **6**, 11.
71 P. R. Salgado, M. E. López-Caballero, M. C. Gómez-Guillén, A. N. Mauri and M. P. Montero, *Food Hydrocolloids*, 2012, **29**, 374–381.
72 K. Chie, *Effect of glycation on ε-polylysine with dextran using maillard reaction on its antimicrobial activity, antioxidant activity, and stability*, Doctoral dissertation, California State Polytechnic University, Pomona, 2022.
73 H. Baniasadi, Z. Fathi, E. Lizundia, C. D. Cruz, R. Abidnejad, M. Fazeli, P. Tammela, E. Kontturi, J. Lipponen and J. Niskanen, *Food Hydrocolloids.*, 2025, **158**, 110525.
74 M. Gallo, G. Arrighi, L. Moreschi, A. Del Borghi, A. Athanassiou and G. Perotto, *ACS Sustainable Chem. Eng.*, 2022, **10**, 13936–13944.
75 S. Wang, W. Wang and H. Yang, *Int. J. Environ. Res. Public Health*, 2018, **15**(10), 2060, DOI: **10.3390/ijerph15102060**.
76 R. Garcia and F. Freire, *J. Cleaner Prod.*, 2014, **66**, 199–209.
77 E. A. R. Zuiderveen, K. J. J. Kuipers, C. Caldeira, S. V. Hanssen, M. K. van der Hulst, M. M. J. de Jonge, A. Vlysidis, R. van Zelm, S. Sala and M. A. J. Huijbregts, *Nat. Commun.*, 2023, **14**, 8521.
78 K. E. Wyer, D. B. Kelleghan, V. Blanes-Vidal, G. Schauberger and T. P. Curran, *J. Environ. Manage.*, 2022, **323**, 116285.

 This journal is © The Royal Society of Chemistry 2025